PHYSICAL REVIEW B **92**, 140407(R) (2015)

Antiferromagnetic order in the pyrochlores $R_2Ge_2O_7$ (R=Er, Yb)

Z. L. Dun,[1] X. Li,[2] R. S. Freitas,[3] E. Arrighi,[3] C. R. Dela Cruz,[4] M. Lee,[5,6] E. S. Choi,[6] H. B. Cao,[4] H. J. Silverstein,[7] C. R. Wiebe,[6,7,8,9] J. G. Cheng,[2] and H. D. Zhou[1,6]

[1]*Department of Physics and Astronomy, University of Tennessee, Knoxville, Tennessee 37996-1200, USA*
[2]*Beijing National Laboratory for Condensed Matter Physics and Institute of Physics, Chinese Academy of Sciences, Beijing 100190, China*
[3]*Instituto de Fisica, Universidade de Sao Paulo, CP 66318, 05314-970 Sao Paulo, SP, Brazil*
[4]*Quantum Condensed Matter Division, Oak Ridge National Laboratory, Oak Ridge, Tennessee 37381, USA*
[5]*Department of Physics, Florida State University, Tallahassee, Florida 32306-3016, USA*
[6]*National High Magnetic Field Laboratory, Florida State University, Tallahassee, Florida 32310-3706, USA*
[7]*Department of Chemistry, University of Manitoba, Winnipeg, Canada MB R3T 2N2*
[8]*Department of Chemistry, University of Winnipeg, Winnipeg, MB, Canada R3B 2E9*
[9]*Canadian Institute for Advanced Research, Toronto, Ontario, Canada M5G 1Z7*

(Received 9 April 2015; revised manuscript received 16 September 2015; published 7 October 2015)

Elastic neutron scattering, ac susceptibility, and specific heat experiments on the pyrochlores $Er_2Ge_2O_7$ and $Yb_2Ge_2O_7$ show that both systems are antiferromagnetically ordered in the Γ_5 manifold. The ground state is a ψ_3 phase for the Er sample and a ψ_2 or ψ_3 phase for the Yb sample, which suggests "Order by Disorder" physics. Furthermore, we unify the various magnetic ground states of all known $R_2X_2O_7$ (R = Er, Yb; X = Sn, Ti, Ge) compounds through the enlarged XY-type exchange interaction $J_\pm$ under chemical pressure. The mechanism for this evolution is discussed in terms of the phase diagram proposed in the theoretical study by Wong *et al.* [Phys. Rev. B **88**, 144402 (2013)].

DOI: 10.1103/PhysRevB.92.140407 PACS number(s): 75.10.Jm, 61.05.fm, 75.40.−s

The pyrochlores $R_2X_2O_7$ (R: rare earth elements; X: transition metals) have been a hot topic due to their emergent physical properties based on the geometrically frustrated lattice [1,2]. Recent interest in pyrochlores is focused on systems with effective spin-1/2 R^{3+} ions [3,4], in which the crystal electric field (CEF) normally introduces a well-isolated Kramers doublet ground state with easy XY planar anisotropy [5,6]. In these XY pyrochlores, the anisotropic nearest neighbor exchange interaction $J_{ex} = (J_{zz}, J_\pm, J_{z\pm}, J_{\pm\pm})$ between the R^{3+} ions, plus the strong quantum spin fluctuations of the effective spin-1/2 moment, stabilize various exotic magnetic ground states [3].

$Er_2Ti_2O_7$ and $Yb_2Ti_2O_7$ are two celebrated examples of the effective spin-1/2 XY pyrochlores. For $Yb_2Ti_2O_7$, the local [111] Ising-like exchange interaction J_{zz} is considerably larger than the XY planar interaction $J_\pm$ [7]. An unconventional first order transition is observed [8], which has been proposed to be a splayed-ferromagnet (SF) state with Yb^{3+} spins pointing along one of the global major axes with a canting angle [9]. For $Er_2Ti_2O_7$, the Er^{3+} spins are energetically favored to lie within the local XY plane due to the dominating $J_\pm$, in which an accidental U(1) degeneracy is preserved in the Hamiltonian at the mean-field level that allows the Er^{3+} spins to rotate continuously in the XY plane [10–13]. Recently, both experimental and theoretical studies suggest that the quantum spin fluctuations lift the U(1) degeneracy with a small gap opening in the spin-wave spectrum and select an antiferromagnetic (AFM) ordering state (ψ_2) as the ground state for $Er_2Ti_2O_7$. This is the so-called "order by disorder" (ObD) mechanism [13–17], in which the ground state is selected through entropic effects. Meanwhile, an alternative CEF-induced energetic selection mechanism is proposed that will likewise result in the ψ_2 state with similar value of the gap [18,19].

These delicate magnetic ground states are fragile and easily affected by perturbations, such as chemical pressure. By replacing the Ti^{4+} sites with the nonmagnetic Sn^{4+} and Ge^{4+} ions, the lattice parameter varies to changes in the exchange interactions. As listed in Table I, for both $Er_2X_2O_7$ and $Yb_2X_2O_7$ series, the Curie temperature and ordering temperature increase with decreasing lattice parameter. Moreover, their magnetic ground states are markedly different. $Er_2Sn_2O_7$ does not show any long-range magnetic ordering down to 50 mK [20] but displays a spin freezing below 200 mK with the AFM Palmer-Chalker (PC) correlations [21]. It is proposed that $Er_2Sn_2O_7$ is approaching the ψ_2/PC phase boundary where the selection of either state is weak [21–23]. $Er_2Ge_2O_7$ shows an AFM ordering [24] that is similar to $Er_2Ti_2O_7$. While a similar SF phase is observed for both $Yb_2Ti_2O_7$ and $Yb_2Sn_2O_7$ [25–27], $Yb_2Ge_2O_7$ strikingly displays AFM ordering at $T_N = 0.61$ K [28]. So far, the exact nature of the magnetic ground states of $Er_2Ge_2O_7$ and $Yb_2Ge_2O_7$ are not clear. Are they also selected by ObD mechanism [29]? More importantly, while the theoretical studies [3,22,23] have made significant efforts to unify the magnetic properties of Yb and Er-XY pyrochlores, unified magnetic phase diagrams have not been experimentally achieved.

In this Rapid Communication, we studied the polycrystalline pyrochlores $Er_2Ge_2O_7$ and $Yb_2Ge_2O_7$ using elastic neutron scattering under magnetic fields, ac susceptibility, and specific heat measurements. We identified a ψ_3 phase for the Er sample and a ψ_2 or ψ_3 phase for the Yb sample[see Figs. 1(e) and 1(f) for their spin configurations], which suggest ObD mechanism. Furthermore, we unified the various magnetic ground states of all studied $R_2X_2O_7$ (R = Er, Yb; X = Sn, Ti, Ge) through the enlarged XY-type exchange interaction $J_\pm$ under chemical pressure. We discussed this general rule in terms of the phase diagram proposed by Wong *et al.* [23].

Experimental details are listed in the Supplemental Material [31]. By comparing the neutron diffraction patterns

TABLE I. Comparison between $Er_2X_2O_7$ and $Yb_2X_2O_7$.

	$Er_2X_2O_7$			$Yb_2X_2O_7$		
X site ion	Sn	Ti	Ge	Sn	Ti	Ge
IR(X^{4+}) (Å)	0.69	0.605	0.53	0.69	0.605	0.53
a (Å)	10.35	10.07	9.88	10.28	10.03	9.83
θ_{CW} (K)	−14	−15.9	−21.9	0.53	0.75	0.9
T_N	∼	1.17	1.41	0.15	0.24	0.62
Order type	∼(AFM)	AFM	AFM	FM	FM	AFM
Reference	[21]	[30]	[24]	[25]	[8]	[28]
Spin state	∼(PC)	ψ_2	ψ_3	SF	SF	$\psi_{2(\text{or }3)}$
Reference	[21]	[14]	This work	[25]	[9]	This work

measured at 3 and 0.3 K [Figs. 1(a) and 1(b)] for $Er_2Ge_2O_7$, several magnetic Bragg peaks, such as (111), (220), (311), etc., are clearly observed at 0.3 K ($<T_N = 1.41$ K). The refinements using the XY-type AFM spin structure in the Γ_5 manifold, either ψ_2 or ψ_3 [Figs. 1(e) and 1(f)], fit these magnetic Bragg peaks well with a magnetic moment of $3.23(6)\mu_B$. In fact, all magnetic phases within the Γ_5 manifold result in the same diffraction pattern and it is impossible to distinguish them in powder samples with zero-field data. Figure 1(d) shows the field dependence of the (220) and (311) Bragg peaks intensities. The details are (i) with $H < 0.15$ T, a magnetic domain alignment results in a quick drop of the

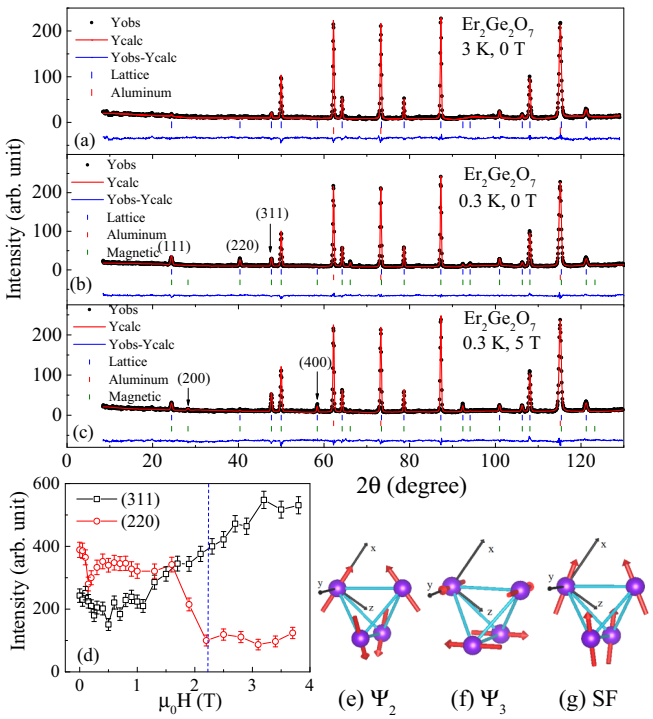

FIG. 1. (Color online) Elastic neutron scattering patterns and Rietveld refinements for $Er_2Ge_2O_7$ at (a) $T = 3$ K and $H = 0$ T, (b) $T = 0.3$ K and $H = 0$ T, and (c) $T = 0.3$ K and $H = 5$ T. (d) The field dependence of the (220) and (311) Bragg peaks intensities measured at $T = 0.3$ K; the critical field H_c is marked as the dashed line. The spin configurations for (e) ψ_2, (f) ψ_3, and (g) SF phases in the local coordination.

(220) peak intensity with increasing field; (ii) between 0.15 and 2 T, the spins gradually rotate with the magnetic field but keep the AFM nature; (iii) around a critical field $H_c = 2$ T, the (220) Bragg peak intensity abruptly drops to a background value, while the (311) Bragg peak intensity continuously increases. This demonstrates that above H_c, $Er_2Ge_2O_7$ enters a spin polarized state. The observed FM (400) and AFM (200) Bragg peaks on the pattern measured at $H = 5$ T [Fig. 1(c)] suggest that this polarized state is similar to the SF state in the Γ_9 manifold. The refinement by assuming one single SF structure with the magnetic field applied along the global z axis [Fig. 1(g)] actually fits the powder average 5 T data well with the Er^{3+} moment as $\vec{M} = (\pm 1.42(2), \pm 1.42(2), 4.40(1))\mu_B$ in the global coordinate frame. The double peak feature of the reported ac susceptibility data for $Er_2Ge_2O_7$ also confirmed the magnetic domain alignment around 0.15 T and the critical field around 2 T [24].

It has been pointed out [14] that (i) for both ψ_2 and ψ_3 states, a multidomain state with equal fraction of six magnetic domains (plotted in the Supplemental Material [31]) at zero field will be expected, which give different intensities of the (220) Bragg peak; (ii) with the applied magnetic field in the $[1\bar{1}0]$ direction, two domains with larger intensity will be selected if the ψ_2 phase is present [10]. This will result in a (220) peak intensity jump, which has been exactly observed for $Er_2Ti_2O_7$ in the single crystal neutron diffraction experiments [10,13,32]; (iii) similarly, if the ψ_3 state is selected, a decrease is expected for the (220) peak intensity since the two domains with lower intensities will be selected. In our neutron powder diffraction experiment by using a pelleted sample, the magnetic field was applied vertically such that it is perpendicular to the scattering plane. Then a similar selection rule would be expected in addition to a powder averaging effect [31]. As shown in Fig. 1(d), the (220) peak intensity drops dramatically from 400 at 0 T to 250 counts at 0.15 T. This result suggests that $Er_2Ge_2O_7$ orders in the ψ_3 phase. However, in order to provide unambiguous evidence for the ψ_3 state, polarized neutron experiments on a single crystal sample are needed.

Figure 2(a) shows the neutron diffraction pattern measured at 0.3 K ($<T_N = 0.62$ K) for $Yb_2Ge_2O_7$. Due to the small magnetic moment of the Yb^{3+} ions, the magnetic Bragg peaks are weak (as shown in the inset). The difference between the 0.3 and 1.6 K patterns [Fig. 2(b)] more clearly shows that the observed magnetic Bragg peaks positions and intensity ratios are very similar to those of $Er_2Ge_2O_7$, which identifies $Yb_2Ge_2O_7$'s ground state as either ψ_2 or ψ_3 in the Γ_5 manifold. Refinements based on these two spin structures give the same Yb^{3+} moment of $1.06(7)\mu_B$, which is consistent with the previous report ($Yb^{3+} \approx 1.15\mu_B$) [33].

With an applied magnetic field on $Yb_2Ge_2O_7$ [Fig. 2(c)], the (220) peak intensity decreases quickly around 0.2 T, which indicates a critical field $H_c \sim 0.2$ T. Upon H_c, the (311) and (400) magnetic Bragg peaks experience a continuous increase, showing a continuous polarization of Yb^{3+} spin towards the direction of the magnetic field. The refinement of the 0.3 K pattern measured under 2 T actually yields a SF state with $\vec{M} = (\pm 0.31(5), \pm 0.31(5), 1.57(9))\mu_B$ in the global coordinate frame. The critical field is also confirmed by the ac magnetization measurement [Fig. 2(d)]. At 75 mK, the ac susceptibility first shows a peak at 0.12 T due to the domain

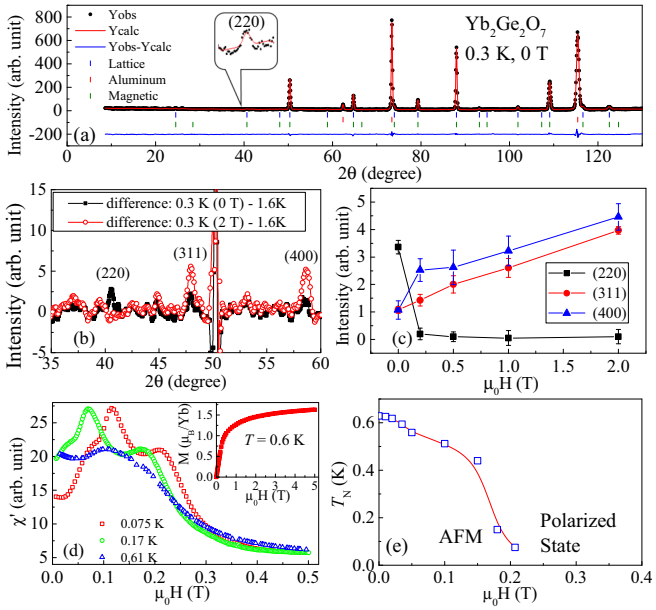

FIG. 2. (Color online) (a) Elastic neutron scattering pattern and Rietveld refinement for $Yb_2Ge_2O_7$ at $T = 0.3$ K and $H = 0$ T. (b) The difference between the patterns measured at 0.3 K (with $H = 0$ and 2 T) and 1.6 K. (c) The field dependence of the (220), (311), and (400) Bragg peaks intensities at 0.3 K. (d) The ac susceptibility of $Yb_2Ge_2O_7$ at different temperatures. Inset: The dc magnetization measured at 0.6 K. (e) The magnetic phase diagram of $Yb_2Ge_2O_7$.

alignment, and then another peak around $H_c = 0.22$ T to enter the polarized state. With increasing temperature, both peaks' positions move to lower fields and finally disappear above T_N. This double peak feature is similar to that of $Er_2Ge_2O_7$ [24]. Along with our previous reported ac susceptibility data on $Yb_2Ge_2O_7$ [28], a magnetic phase diagram is plotted in Fig. 2(e). However, due to the weak magnetic signal at (220) and the small H_c, it is difficult to study how exactly this domain alignment affects the (220) peak intensity, which obstructs us from distinguishing between ψ_2 and ψ_3. One noteworthy feature is that the dc magnetization measured at 0.6 K for $Yb_2Ge_2O_7$ reaches $1.6\mu_B$ at 5 T. This value is consistent with that of $Yb_2Ti_2O_7$ and confirms the similar CEF scheme between the Ge and Ti samples [33].

The selection of either the ψ_2 or ψ_3 phase breaks the continuous U(1) symmetry, which requires a pseudo-Goldstone mode with a spin-wave gap below T_N. For $Er_2Ti_2O_7$, the inelastic neutron scattering has confirmed the existence of this gap (~50 μeV) [17]. Meanwhile, the specific heat data can reveal the information of this gap. Figure 3(a) shows the electronic magnetic specific heat (C_m) of $Yb_2Ge_2O_7$ [31]. Below T_N, C_m follows an almost prefect T^3 behavior down to 0.2 K, as the red dashed line shows. However, it is obvious that C_m deviates from this straight T^3 line to a lower value below 0.2 K. In contrast to a Goldstone mode where the C_m strictly follows a T^3 law, the gap that exists in the pseudo-Goldstone mode will multiply a component $I_\Delta(T)$ to T^3, which is temperature dependent only in the temperature region that is comparable to the energy gap Δ. The relationship between the C_m and Δ has already been derived in the supporting material of Ref. [13]. Here we rewrite it as

$$C_m^\Delta = \frac{\mathcal{N}_A k_B^4 \pi^2 a^3}{120\overline{v}^3}\left(\frac{15}{16\pi^4}\int_0^\infty dX \frac{X^2(X^2+\delta^2)}{\sinh^2\frac{\sqrt{X^2+\delta^2}}{2}}\right)T^3$$
$$= AI_\Delta(T)T^3, \quad (1)$$

where $\mathcal{N}_A$ is the Avogadro constant, k_B is the Boltzmann constant, a is the lattice constant, $\overline{v}$ is the geometric mean of magnon velocity, $X = \beta\tilde{k}$, and $\delta = \beta\Delta$ (dimensionless). The integration $I_\Delta(T)$ can be evaluated numerically with a given Δ. $I_\Delta(T)$ approaches a unity at high temperatures but decreases quickly when k_BT is comparable to Δ, which leads the deviation of the C_m^Δ from the T^3 behavior at low temperatures. The best fit of the measured C_m to Eq. (1) with the Δ and A as two variables [blue line in Fig. 3(a)] yields the $\Delta = 24$ μeV and $A = 15.67$ J K^{-4} mol^{-1}, which corresponds to $\overline{v} = 45.8$ m/s.

Similar analysis of the C_m for $Er_2Ge_2O_7$ [Fig. 3(b)] yields a spin-wave gap $\Delta = 45$ μeV with $A = 1.85$ J K^{-4} mol^{-1}(corresponds to $\overline{v} = 132$ m/s). One noticed feature is that at high temperatures, C_m follows a $T^{2.72}$ (not strict T^3) behavior. This could be due to the error bar introduced by the low temperature nuclear Schottky anomaly subtraction.

With the decreasing lattice parameter or the increasing chemical pressure through the Sn to Ti to Ge samples, the magnetic ground states change accordingly (Table I). Given the fact that in these XY pyrochlores, the J_{ex} dominate the magnetic properties, the chemical pressure can finely tune the J_{ex} to lead to various magnetic ground states. This change of J_{ex} is supported by the systematic changes of the Curie temperature and ordering temperature for XY pyrochlores listed in Table I. Most strikingly, here we experimentally confirm an AFM $\psi_{2\text{ or }3}$ phase in Yb pyrochlores despite the apparently different dominant exchange interactions between Yb and Er pyrochlores (Ising-like J_{zz} for Yb pyrochlores and the XY planar $J_\pm$ for Er pyrochlores). This finding indicates there are general rules to unify the various magnetic ground states of all effective spin-1/2 pyrochlores.

Recent theoretical studies have made significant efforts to unify the magnetic ground states of the XY pyrochlores. Wong *et al.* [23] have scaled the J_{ex} by $J_\pm$ as three variables ($J_{zz}/J_\pm$, $J_{z\pm}/J_\pm$, $J_{\pm\pm}/J_\pm$) and calculated a two-dimensional magnetic

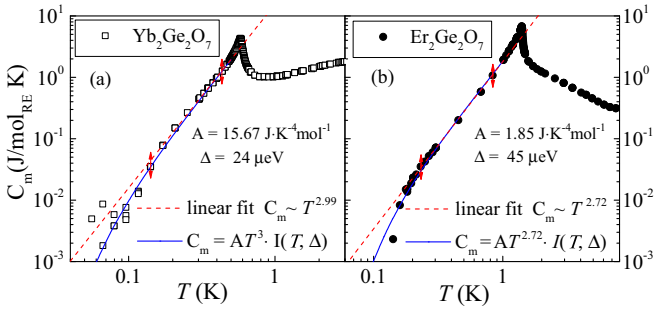

FIG. 3. (Color online) The electronic magnetic specific heat C_m for (a) $Yb_2Ge_2O_7$ and (b) $Er_2Ge_2O_7$. The red dashed lines show linear fits of the arrow-marked regions and the blue solid lines show fits considering the spin-wave gap.

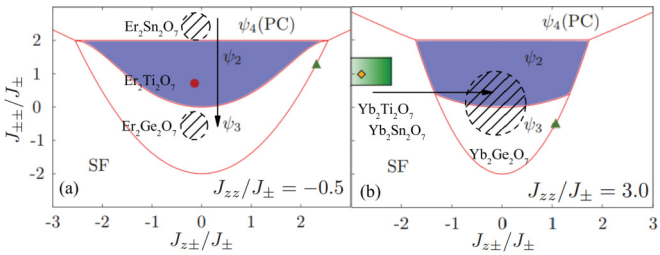

FIG. 4. (Color online) Magnetic ground state phase diagrams for (a) $Er_2X_2O_7$ series and (b) $Yb_2X_2O_7$ series adopted from Ref. [23]. The dashed areas are just for the illustration purposes. The trends for the chemical pressure effects are shown as the direction of the arrows.

phase diagram with the fixed ratio of $J_{zz}/J_\pm$, which contains continuous phase boundaries among the PC, SF, ψ_2, and ψ_3 phases (the phase boundary between ψ_2 and ψ_3 is determined through ObD). By adopting the exchange interaction values obtained from the inelastic neutron scattering measurements, they successfully located the two Ti samples ($J_{zz}/J_\pm \approx -0.5$, $J_{z\pm}/J_\pm \approx 0$, $J_{\pm\pm}/J_\pm \approx 1.0$ for $Er_2Ti_2O_7$ and $J_{zz}/J_\pm \approx 3.0$, $J_{z\pm}/J_\pm \approx -2.7$, $J_{\pm\pm}/J_\pm \approx 1.0$ for $Yb_2Ti_2O_7$) in the ψ_2 and SF phase, respectively. Although we are short of knowledge of the exchange interaction values of other XY pyrochlores, here we located them in the $J_{zz}/J_\pm = -0.5$ and the $J_{zz}/J_\pm = 3.0$ phase diagrams adopted from Ref. [23]. This is based on three facts: (i) the phase diagram areas and boundaries are similar to each other over a wide range value of $J_{zz}/J_\pm$; (ii) the ratio of $J_{zz}/J_\pm$ will not dramatically change for each pyrochlore series due to the similar ion anisotropy; (iii) for both compounds, no additional transition or anomaly is observed from T_N to the lowest temperature of 50 mK either from the ac susceptibility or the specific heat measurement. This suggests that the 0.3 K spin structure as seen by neutrons reflect the nature of its magnetic ground state ($T = 0$), which in principle could be different from the state selected near the criticality ($T \leqslant T_c$) [12,29]. As shown in Fig. 4, with increasing chemical pressure, two general trends are obvious: (i) the ground state moves downwards from the PC state in $Er_2Sn_2O_7$ to ψ_2 in $Er_2Ti_2O_7$ and then ψ_3 in $Er_2Ge_2O_7$ for the Er pyrochlores in the $J_{zz}/J_\pm = -0.5$ phase diagram; (ii) the ground states move rightwards from the SF state of $Yb_2Ti_2O_7$ to the ψ_2 or ψ_3 region of $Yb_2Ge_2O_7$ in the $J_{zz}/J_\pm = 3.0$ phase diagram.

These two trends can be successfully unified by the scenario that the increasing chemical pressure enhances $J_\pm$. For Er pyrochlores with dominant XY-type interactions, J_{zz} and $J_{z\pm}$ will take small values. Therefore, the increasing $J_\pm$ will primarily decrease the ratio of $J_{\pm\pm}/J_\pm$ to result in a downwards movement of the ground state. On the other hand, for Yb pyrochlores with dominant local [111] Ising-like interactions, $J_\pm$ and $J_{\pm\pm}$ will take small values. Therefore, the increasing $J_\pm$ will mainly decrease the ratio of $J_{z\pm}/J_\pm$ to result in a rightwards shift of the ground state to reach the AFM state for $Yb_2Ge_2O_7$. Although without the values of the exchange interactions for all XY pyrochlores, we cannot conclude the increase of the $J_\pm$ as the only reason for the change of ground states, the comparison between the reported $J_\pm$ values of $Er_2Sn_2O_7$ ($J_\pm = 13.5\,\mu$eV) [21] and $Er_2Ti_2O_7$ ($J_\pm = 65\,\mu$eV) [13] supports our proposed scenario.

Similar to $Er_2Ti_2O_7$, the debate arises over what is the microscopic mechanism that breaks the continuous U(1) symmetry and selected the ordered ground state. The selection of different ground states in $Er_2Ti_2O_7$ (ψ_2) and $Er_2Ge_2O_7$ (ψ_3) seems to favor the ObD scenario since the selection comes from the quantum fluctuations, which is delicately tuned by the exchange parameters J_{ex} [13–16] (Fig. 4). Future experiments are needed to explore the potential quantum fluctuations and the possible selection differences between $T \leqslant T_c$ and $T = 0$, which are predicted theoretically within the ObD scenario [12,29]. On the other hand, it still remains a theoretical challenge for the CEF-induced energetic selection scenario to explore the possible existence of different spin states, except for the proposed ψ_2 phase for Er pyrochlores [18,19,21]. Furthermore, it is noticed that the values of magnon mean velocity and the gap in $Yb_2Ge_2O_7$ ($\overline{v} = 45.8$ m/s, $\Delta = 24\,\mu$eV) are both smaller than that of $Er_2Ge_2O_7$ ($\overline{v} = 132$ m/s, $\Delta = 45\,\mu$eV), which is consistent with the ObD mechanism. A smaller $\overline{v}$ suggests a softer low-lying mode in the spin-wave spectrum that will result in a smaller energy difference of spin-wave spectrum between the ψ_2 and ψ_3 phases [13], for which a smaller gap is expected.

Z.L.D. and H.D.Z. acknowledge the support of Grant No. NSF-DMR-1350002. R.S.F. acknowledges support from CNPq (Grant No. 400278/2012-0). X.L and J.G.C. are supported by the NSFC (Grant No. 11304371) and the Strategic Priority Research Program (B) of the Chinese Academy of Sciences (Grant No. XDB07020100). E.S.C. acknowledges the support of NSF (Grant No. DMR-1309146). H.J.S. acknowledges support through NSERC (the Vanier program). C.R.W. acknowledges NSERC, CFI, the CRC program (Tier II), and CIFAR. The work at NHMFL is supported by Grant No. NSF-DMR-1157490 and the State of Florida and by the additional funding from NHMFL User Collaboration Support Grant. The work at ORNL High Flux Isotope Reactor was sponsored by the Scientific User Facilities Division, Office of Basic Energy Sciences, US Department of Energy.

[1] J. S. Gardner, M. J. P. Gingras, and J. E. Greedan, Rev. Mod. Phys. **82**, 53 (2010).
[2] L. Balents, Nature (London) **464**, 199 (2010).
[3] L. Savary and L. Balents, Phys. Rev. Lett. **108**, 037202 (2012).
[4] S. Onoda, J. Phys.: Conf. Series **320**, 012065 (2011).
[5] J. D. M. Champion and P. C. W. Holdsworth, J. Phys.: Condens. Matter **16**, S665 (2004).
[6] H. B. Cao, A. Gukasov, I. Mirebeau, P. Bonville, C. Decorse, and G. Dhalenne, Phys. Rev. Lett. **103**, 056402 (2009).
[7] K. A. Ross, L. Savary, B. D. Gaulin, and L. Balents, Phys. Rev. X **1**, 021002 (2011).
[8] J. A. Hodges, P. Bonville, A. Forget, A. Yaouanc, P. Dalmas de Reotier, G. Andre, M. Rams, K. Krolas, C. Ritter,

P. C. M. Gubbens, C. T. Kaiser, P. J. C. King, and C. Baines, Phys. Rev. Lett. **88**, 077204 (2002).

[9] L. J. Chang, S. Onoda, Y. Su, Y. J. Kao, K. D. Tsuei, Y. Yasui, K. Kakurai, and M.R. Lees, Nat. Commun. **3**, 992 (2012).

[10] J. D. M. Champion, M. J. Harris, P. C. W. Holdsworth, A. S. Wills, G. Balakrishnan, S. T. Bramwell, E. Čižmár, T. Fennell, J. S Gardner, J. Lago, D. F. McMorrow, M. Orendáč, A. Orendáčová, D. McK. Paul, R. I. Smith, M. T. F. Telling, and A. Wildes, Phys. Rev. B **68**, 020401(R) (2003).

[11] J. P. C. Ruff, J. P. Clancy, A. Bourque, M. A. White, M. Ramazanoglu, J. S. Gardner, Y. Qiu, J. R. D. Copley, M. B. Johnson, H. A. Dabkowska, and B. D. Gaulin, Phys. Rev. Lett. **101**, 147205 (2008).

[12] B. Javanparast, A. G. R. Day, Z. Hao, and M. J. P. Gingras, Phys. Rev. B **91**, 174424 (2015).

[13] L. Savary, K. A. Ross, B. D. Gaulin, J. P. C. Ruff, and Leon Balents, Phys. Rev. Lett. **109**, 167201 (2012).

[14] A. Poole, A. S. Wills, and E. E. Lelievre-Berna, J. Phys.: Condens. Matter **19**, 452201 (2007).

[15] P. A. McClarty, P. Stasiak, and M. J. P. Gingras, Phys. Rev. B **89**, 024425 (2014).

[16] M. E. Zhitomirsky, M. V. Gvozdikova, P. C. W. Holdsworth, and R. Moessner, Phys. Rev. Lett. **109**, 077204 (2012).

[17] K. A. Ross, Y. Qiu, J. R. D. Copley, H. A. Dabkowska, and B. D. Gaulin, Phys. Rev. Lett. **112**, 057201 (2014).

[18] S. Petit, J. Robert, S. Guitteny, P. Bonville, C. Decorse, J. Ollivier, H. Mutka, M. J. P. Gingras, and I. Mirebeau, Phys. Rev. B **90**, 060410(R) (2014).

[19] P. A. Mcclarty, S. H. Curnoe, and M. J. P. Gingras, J. Phys.: Conf. Ser. **145**, 012032 (2009).

[20] P. M. Sarte, H. J. Silverstein, B. T. K. Van Wyk, J. S. Gardner, Y. Qiu, H. D. Zhou, and C. R. Wiebe, J. Phys.: Condens. Matter **23**, 382201 (2011).

[21] S. Guitteny, S. Petit, E. Lhotel, J. Robert, P. Bonville, A. Forget, and I. Mirebeau, Phys. Rev. B **88**, 134408 (2013).

[22] H. Yan, O. Benton, L. D. C. Jaubert, and N. Shannon, arXiv:1311.3501.

[23] A. W. C. Wong, Z. Hao, and M. J. P. Gingras, Phys. Rev. B **88**, 144402 (2013).

[24] X. Li, W. M. Li, K. Matsubayashi, Y. Sato, C. Q. Jin, Y. Uwatoko, T. Kawae, A. M. Hallas, C. R. Wiebe, A. M. Arevalo-Lopez, J. P. Attfield, J. S. Gardner, R. S. Freitas, H. D. Zhou, and J.-G. Cheng, Phys. Rev. B **89**, 064409 (2014).

[25] A. Yaouanc, P. Dalmas de Reotier, P. Bonville, J. A. Hodges, V. Glazkov, L. Keller, V. Sikolenko, M. Bartkowiak, A. Amato, C. Baines, P. J. C. King, P. C. M. Gubbens, and A. Forget, Phys. Rev. Lett. **110**, 127207 (2013).

[26] Z. L. Dun, E. S. Choi, H. D. Zhou, A. M. Hallas, H. J. Silverstein, Y. Qiu, J. R. D. Copley, J. S. Gardner, and C. R. Wiebe, Phys. Rev. B **87**, 134408 (2013).

[27] J. Lago, I. Zivkovic, J. O. Piatek, P. Alvarez, D. Huvonen, F. L. Pratt, M. Diaz, and T. Rojo, Phys. Rev. B **89**, 024421 (2014).

[28] Z. L. Dun, M. Lee, E. S. Choi, A. M. Hallas, C. R. Wiebe, J. S. Gardner, E. Arrighi, R. S. Freitas, A. M. Arevalo-Lopez, J. P. Attfield, H. D. Zhou, and J. G. Cheng, Phys. Rev. B **89**, 064401 (2014).

[29] L. D. C. Jaubert, O. Benton, J. G. Rau, J. Otimaa, R. R. P. Singh, N. Shannon, and M. J. P. Gingras, arXiv:1505.05499.

[30] P. Dalmas de Réotier, A. Yaouanc, Y. Chapuis, S. H. Curnoe, B. Grenier, E. Ressouche, C. Marin, J. Lago, C. Baines, and S. R. Giblin, Phys. Rev. B **86**, 104424 (2012).

[31] See Supplemental Material at http://link.aps.org/supplemental/10.1103/PhysRevB.92.140407 for details of sample synthesis, experimental setups, specific heat subtraction, and magnetic domain alignment analysis.

[32] H. B. Cao, I. Mirebeau, A. Gukasov, P. Bonville, and C. Decorse, Phys. Rev. B **82**, 104431 (2010).

[33] J. A. Hodges, P. Bonville, A. Forget, M. Rams, K. Krolas, and G. Dhalenne, J. Phys.: Condens. Matter **13**, 9301 (2001).